Supporting Information for

"Are remote sensing evapotranspiration models reliable across South American climates and ecosystems?"

D. C. D. Melo[1], J. A. A. Anache[2], E. Wendland[3], V. P. Borges[1], D. Miralles[4], B. Martens[4], J. B. Fisher[5], R. L. B. Nóbrega[6], A. Moreno[7], O. M. R. Cabral[8], T. R. Rodrigues[2], B. Bezerra[9,10], C. M. S. Silva[9,10], A. A. Meira Neto[11], M. S. B. Moura[12], T. V. Marques[10], S. Campos[10], J. S. Nogueira[13], R. Rosolem[14], R. Souza[15], A. C. D. Antonino[16], D. Holl[17], M. Galleguillos[18], J. F. Pérez-Quezada[18,19], A. Verhoef[20], L. Kutzbach[17], J. R. S. Lima[21], E. S. Souza[22], M. I. Gassman[23,24], C. F. Pérez[23,24], N. Tonti[23], G. Posse[25], D. Rains[4], and P. T. S. Oliveira[2]

[1]Federal University of Paraíba, Areia, PB, Brazil

[2]Federal University of Mato Grosso do Sul, Campo Grande, MS, Brazil

[3]Department of Hydraulics and Sanitary Engineering, University of São Paulo, São Carlos, SP, Brazil

[4]Hydro-Climate Extremes Lab (H-CEL), Ghent University, Coupure Links 653, 9000 Ghent, Belgium

[5]Jet Propulsion Laboratory, California Institute of Technology, Pasadena, CA, USA

[6]Department of Life Sciences, Imperial College London, UK

[7]Numerical Terradynamic Simulation Group, University of Montana, Missoula, MT, USA

[8]Brazilian Agricultural Research Corporation, Embrapa Meio Ambiente, Jaguariúna, SP, Brazil

[9]Department of Atmospheric and Climate Sciences, Federal University of Rio Grande do Norte, Natal, RN, Brazil

[10]Climate Sciences Graduate Program, Federal University of Rio Grande do Norte, Natal, RN, Brazil

[11]Department of Hydrology and Atmospheric Sciences, The University of Arizona

[12]Brazilian Agricultural Research Corporation – Embrapa Tropical Semi-arid, Petrolina, PE, Brazil

[13]Federal University of Mato Grosso, Cuiabá, MT, Brazil

[14]University of Bristol, BS7 8PD, UK

[15]Department of Biological and Agricultural Engineering, Texas A&M University, College Station, TX, USA

[16]Department of Nuclear Energy, Federal University of Pernambuco, Recife, PE, Brazil

[17]Center for Earth System Research and Sustainability (CEN), Universität Hamburg, Hamburg, Germany

[18]Department of Environmental Science and Renewable Natural Resources, University of Chile, Santiago, Chile

[19]Institute of Ecology and Biodiversity, Santiago, Chile

[20]Department of Geography and Environmental Science, The University of Reading, Reading, UK

[21]Federal University of the Agreste of Pernambuco, Garanhuns, PE, Brazil

[22]Federal Rural University of Pernambuco, Serra Talhada, PE, Brazil

[23]Department of Atmospheric and Ocean Sciences, FCEN - UBA. Buenos Aires, Argentina

[24]National Council for Scientific and Technical Research, (CONICET), Argentina

[25]Instituto de Clima y Agua. Instituto Nacional de Tecnología Agropecuaria (INTA), Buenos Aires, Argentina

Contents

1. Text S1.0 to S3.0
2. Figures S1 to S11
3. Tables S1 to S3

S1.0 Study area – Biomes

The tropical & subtropical moist broadleaf forests, i.e. TSMBF, cover approximately 50% of the South American territory. This biome is mainly characterized by a warm climate and high rainfall rates. ET in this region is responsible for generating ~30% of the atmospheric moisture that precipitates in the Amazon basin [*Eltahir and Bras*, 1994]. The dry seasonal forests, i.e. TSDBF, are located mostly in the center (Bolivia) and east (Brazilian semi-arid region) of South America; here mean rainfall variability is temporally and spatially high, with pronounced dry seasons that can extend up to 10 months. The biome that encompasses grasslands, savannas, and shrublands, i.e. TSGSS is the second largest biome in South America. This biome has a high concentration of endemic species whose habitats have experienced exceptional losses, therefore many areas of this biome are part of the global biodiversity hotspots for conservation [*Myers et al.*, 2000]. The wetlands, i.e. FBS, host a vast diversity of aquatic and palustrine vegetation [*Junk et al.*, 2006a,b] and provide crucial ecosystem services to the Pantanal (the largest FGS's ecoregion) [*Costanza et al.*, 1997]. FBS are completely surrounded by grasslands, savannas & shrublands, and dry forests. The temperate forests, i.e. TMBF, are located in southern Chile and Argentina. This region contains the Central Chile biodiversity hotspot [*Myers et al.*, 2000]. Mean annual temperature decreases from north to south and from low to high altitudes in the Andes. Within this biome, peatland ecosystems cover most of the area (440,000 km^2, *Arroyo et al.* [2005]) in the southernmost part of South America and along the Pacific coast of Chile.

S2.0 Gap filling of meteorological data

Relative humidity (RH) and vapor pressure (e_a) records are the most common missing variables among the tower data. Missing e_a values were filled using RH and saturated air vapor pressure (e_{sat}) calculated from Tetens' equation [*Tetens*, 1930]. Missing RH values

Corresponding author: Davi Diniz Melo, melo.dcd@gmail.com

were filled accordingly, given that e_a and temperature (T) are available at that day or 30-min interval. Days without T records were discarded. Missing atmospheric pressure (P_{atm}) values were estimated from ground elevation at the tower sites using equation 7 from the FAO-56 manual [*Allen et al.*, 1998].

S3.0 Results and Discussion

ET partitioning

Greater insight into model-based ET partitioning can be gained by comparing our results with other estimates from the literature. Previous model-based estimates using the Gash model [*Gash et al.*, 1995; *Valente et al.*, 1997] for USR (sugar cane) and PDG (woodland savanna) showed that E_{int} accounts for ~10% of ET [*Cabral et al.*, 2012, 2015]. For USR, all three models limited $E_{int}/ET < 10\%$; with PM-MOD offering a mean estimate (~9%) closest to the estimates cited above, and GLEAM presenting the lowest value of E_{int}/ET (<2%). While GLEAM estimated $E_{soil}/ET \approx 5\%$, PM-MOD and PT-JPL estimates (20 and 30%, respectively) agreed better with the 20–40% reported by [*Denmead et al.*, 1997] for two sugar cane fields in Australia. For the EUC site, interception estimates from GLEAM (~10%) are much closer to the $E_{int}/ET \approx 13\%$ reported by *Cabral et al.* [2010], when compared to ~25% estimated by PT-JPL and PM-MOD. For PDG, PT-JPL produced an interception ratio (7% of ET) closest to the $E_{int}/ET = 8\%$ reported by *Cabral et al.* [2015] when compared to GLEAM ($E_{int}/ET = 13\%$) and PM-MOD ($E_{int}/ET = 17\%$). The transpiration fractions (E_{trans}/ET) simulated in this study for the sites in dry regions were mostly higher (>75%) than the range (50–80%) found in several studies by *Jasechko et al.* [2013] (Table 1 in the main text). However, $E_{trans}/ET > 75\%$ for the Brazilian semi-arid areas are reasonable during the rainy season, when about 70% of the annual ET occurs [*Mutti et al.*, 2019; *Marques et al.*, 2020].

All models found practically negligible values of E_{int} (<2% of ET) in three Brazilian semi-arid sites (CAA, CST, and ESEC), despite the fact that previous studies showed that interception loss for native seasonally dry forests (as CAA and CST) accounts for ~10% of ET [*de Queiroz et al.*, 2020]. Regarding ET partitioning from croplands (K77, USR, EUC, GRO, BAL), we found E_{trans}/ET ranging from 85-93% (GLEAM), 46-63% (PT-JPL), and 22-76% (PM-MOD). Hence, the partitioning simulated by GLEAM agrees with previous studies showing that E_{trans} tends to be high in croplands (70–90% of ET), even under low

LAI conditions [*Zhou et al.*, 2016; *Wei et al.*, 2017; *Stoy et al.*, 2019]. Despite the wide variability of E_{trans}/ET among models, the overall predictive skill was satisfactory, thus not associated with their capability to correctly estimate each ET component individually.

Impact of correcting *G*

The impact of the correction of G in the energy balance, thus in the estimation of the observed ET ($= Rn - G - H$), is addressed here. Most Fluxnet-type datasets do not offer soil moisture and soil temperature data, hence correction of G is possible only for a reduced number of validation tower sites. At daily scales, in particular under densely vegetated areas, G is often negligible. The grass sites included in this study lack the data required for correcting G. Therefore, we select the GRO tower (soybean) to assess the role of G in the model metrics. In Figure S8, we show the metrics when tower ET is calculated using G directly measured by soil heat flux plates below the surface (raw G, black dots) and when the corrected G is used (G surface , red dots), i.e. when heat storage above the plate has been taken into account. As shown in Fig S9, no significant change was noted in R^2, $PBIAS$ or $RMSE$; and in most cases the correction caused a deterioration in the metrics. The largest changes were:

- GLEAM: R^2 decreased from 0.79 to 0.74;
- PM-MOD: PBIAS increased from -4.59 to 2.07%
- PT-JPL: RMSE increased from 0.83 to 0.9 mm d^{-1}

Diagnosis

Some factors, e.g. those relating to tower location and the surrounding environment, can also affect model performances. A likely cause for model-observation mismatch, for instance at site K77, could be the heterogeneity of the fluxes measured by the towers [*Bai et al.*, 2015]. Previous studies have shown that land cover heterogeneity may induce some variations in the footprint [*Chen et al.*, 2009]. In the case of the K77 site, the footprint is estimated to extend up to 200 m away from the mast, based on crop and flux sensor heights; however, high resolution images of the K77 surroundings reveal a certain heterogeneity (remnant of forest and shrubs) within a 130-m radius around the tower. Depending on wind speed and direction, tower measurements for this site could therefore be affected by non-crop fluxes.

Aside from patch-scale heterogeneities, there is also the possibility that the 250-m MODIS pixel is returning a mixed response of different types of vegetation within it (sub-pixel spatial heterogeneity), which has been shown to compromise model performance [*Fisher et al.*, 2008; *Mu et al.*, 2011; *Nagler et al.*, 2005; *McCabe et al.*, 2016; *Fisher et al.*, 2020]. "Mixed" pixels of croplands have been shown to be problematic, especially when the VI adopted is EVI [e.g., *Wardlow et al.*, 2007]. In this regard, $NDVI$ might present a certain advantage as it has been shown to better capture the changes in the green biomass level, making it more sensitive to sudden changes among crops in the senescence phase, whereas EVI would be more suitable for mapping crops at the peak phase [*Embry and Nothnagel*, 1994; *Wardlow et al.*, 2007].

Therefore, the mismatch between ET_{sim} and ET_{obs} for K77 site are probably linked to the VI adopted here. An alternative for future work would be to use even higher spatial resolution VNIR/NDVI data than the 250 m MODIS data. Examples include 10-m Sentinel-2 $NDVI$ or 3-m Planet $NDVI$. For instance, *Aragon et al.* [2018] used 3-m Planet NDVI to produce ultra high resolution ET using PT-JPL. Another promising way forward is the 70-m ECOSTRESS ET data (e.g., Figure S11), which enables a closer alignment to eddy covariance footprints [*Fisher et al.*, 2020]. The land cover representativity issue is even worse in the case of GLEAM that uses microwave VOD data for vegetation phenology, a much coarser product. As for the EUC site (~500-m footprint), the plantation border is at a sufficient distance from the tower (~2 km), compared to the surface heterogeneities encountered for the other sites, and occupies multiple MODIS pixels. Hence none of the problems mentioned above are reasonable explanations for the model overprediction at that site in the dry period. Moreover, EVI data from MODIS captured the vegetation variability during transition in terms of amplitude but we noticed a lag between ET_{obs} and EVI (Figure S9). A similar pattern was reported by [*Fisher et al.*, 2008] while validating PT-JPL against ET_{obs} for a savanna tower.

In the case of PT-JPL model estimates at the EUC site, the model's higher sensitivity to *Rn* than to *RH* seems to be a plausible explanation for the model performance (Figure 5; Figure S9). In the PT-JPL model, *RH* affects ET indirectly, through the soil moisture constraint and interception loss. Conversely, influence of *Rn* is indirect: a fraction of it is used to compute all three ET components and it affects the temperature which, in turn, is used to calculate the plant temperature constraint [*Fisher et al.*, 2008]. Moreover, *Rn* has a direct effect on ET as it controls the potential ET in the PT equation. Both the soil moisture and

the plant temperature constraints are positively correlated with modelled ET and they have been shown to be the most sensitive parameters in the PT-JPL model, potentially resulting in ~20% of model uncertainty [*García et al.*, 2013]. Although the RH-dependent constraint presented a larger variability at the EUC site, it tended to follow ET_{obs} variability whereas the Rn-indirectly-dependent constraint remained constant at its maximum value (one) during the months during which overprediction occurred.

The performance of the PM-based models observed here might have been affected by the uncertainties in the estimation of site-specific properties, as we used the leaf conductances (as well as other parameters) from the Biome Properties Look-Up Table in [*Mu et al.*, 2011], instead of calibrating them for the selected sites. As noted by *Ershadi et al.* [2015], the parameterisation seems to be crucial for PM modes. Therefore, a clear path for improving PM-based models over South America is to include its towers for calibrating the biome specific parameters (e.g., potential stomatal conductance, surface conductance etc) in order to make them more representative and account for their inter-continental variability. Moreover, *Mu et al.* [2011] also acknowledged that values of LAI/f_{PAR} from MODIS may introduce a bias in ET estimates, which may explain the systematic errors at some sites (e.g., CAA, FM, K83).

Regarding the PM-VI model, we found it to be the model with the largest variability ($0 < R^2 < 0.85, 0.15 < m < 1.25, 0 < \rho < 0.98$) in performance among the selected towers. Because this model consists of a combination of ETo and an EVI-based crop coefficient, we would expect it to perform best at crop sites. Although that was true for some sites (EUC and USR), PM-VI had the poorest performances at most sites with an aridity index > 1.2. Moreover, the model was capable of estimating ET for non-crop areas, with good predictive skills found at sites with moist forest (K34), mixed forest (FM), woodland savanna (PDG), and two permanent wetland sites (TF1 and TF2). It is interesting to note the contrasting behaviour of the PM-based models. While the PM-MOD is much more complex than PM-VI, the latter outperforms the former at some sites (e.g., TF1 and TF2). This is most likely caused by the fact that PM-MOD has not been calibrated for the flux towers considered here, unlike PM-VI.

Figures S1-10

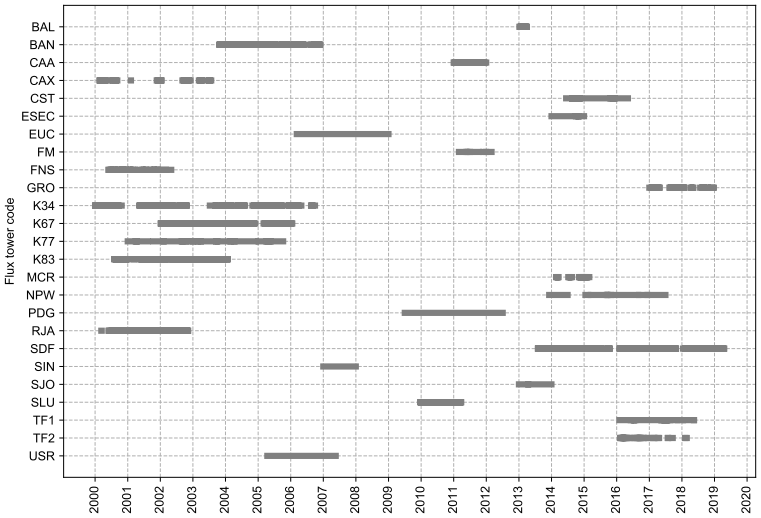

Figure 1. Latent heat flux data availability at individual flux towers.

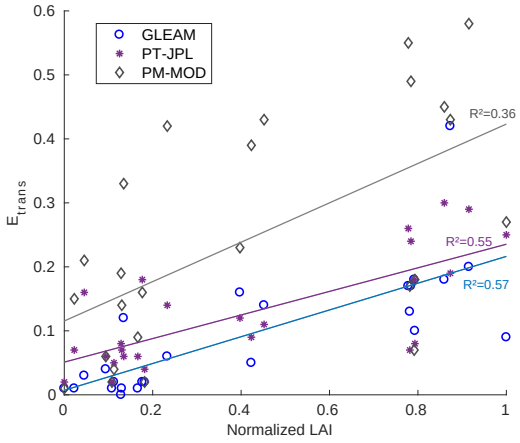

Figure 2. Relationship between E_{int} and LAI for GLEAM, PT-JPL and PM-MOD.

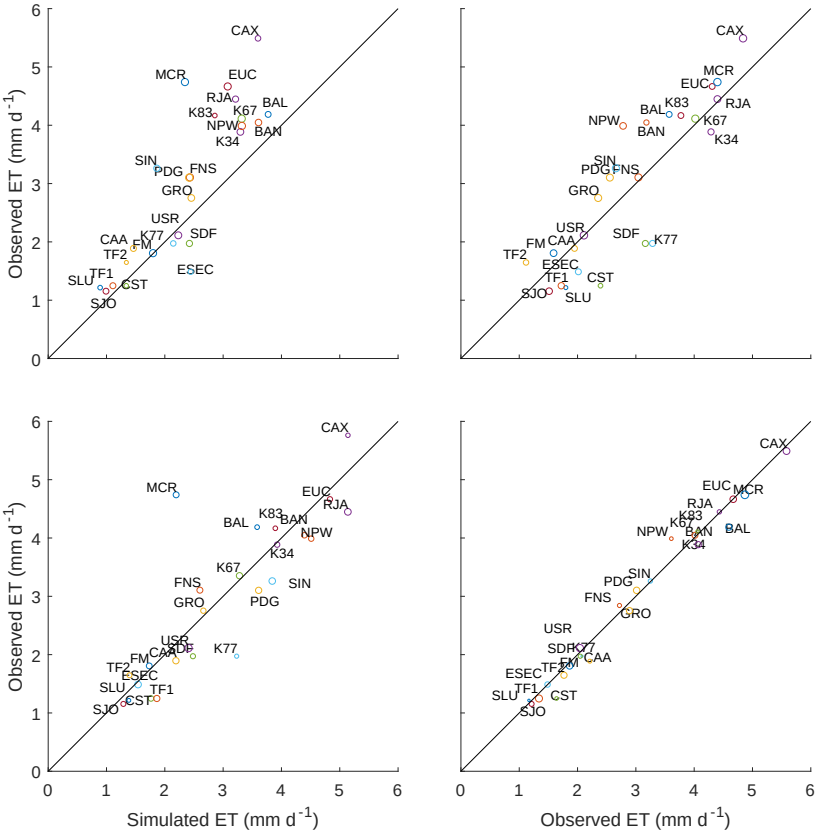

Figure 3. Comparison of mean observed and simulated ET. Circle sizes are proportional to individual model R^2.

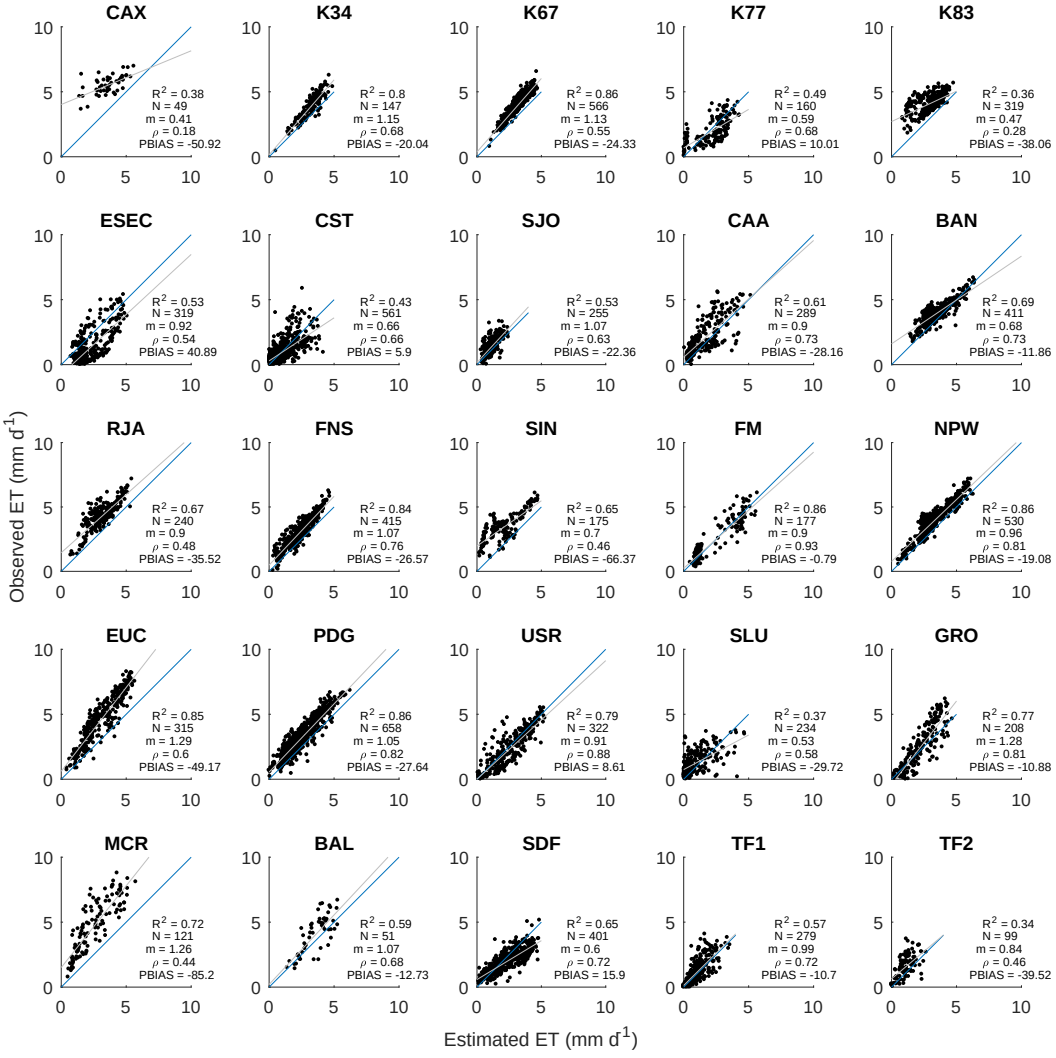

Figure 4. Comparison between observed and simulated ET from GLEAM. N = sample size; R^2= determination coefficient, m = slope of the least squares regression line, ρ = concordance correlation coefficient, PBIAS = percent bias.

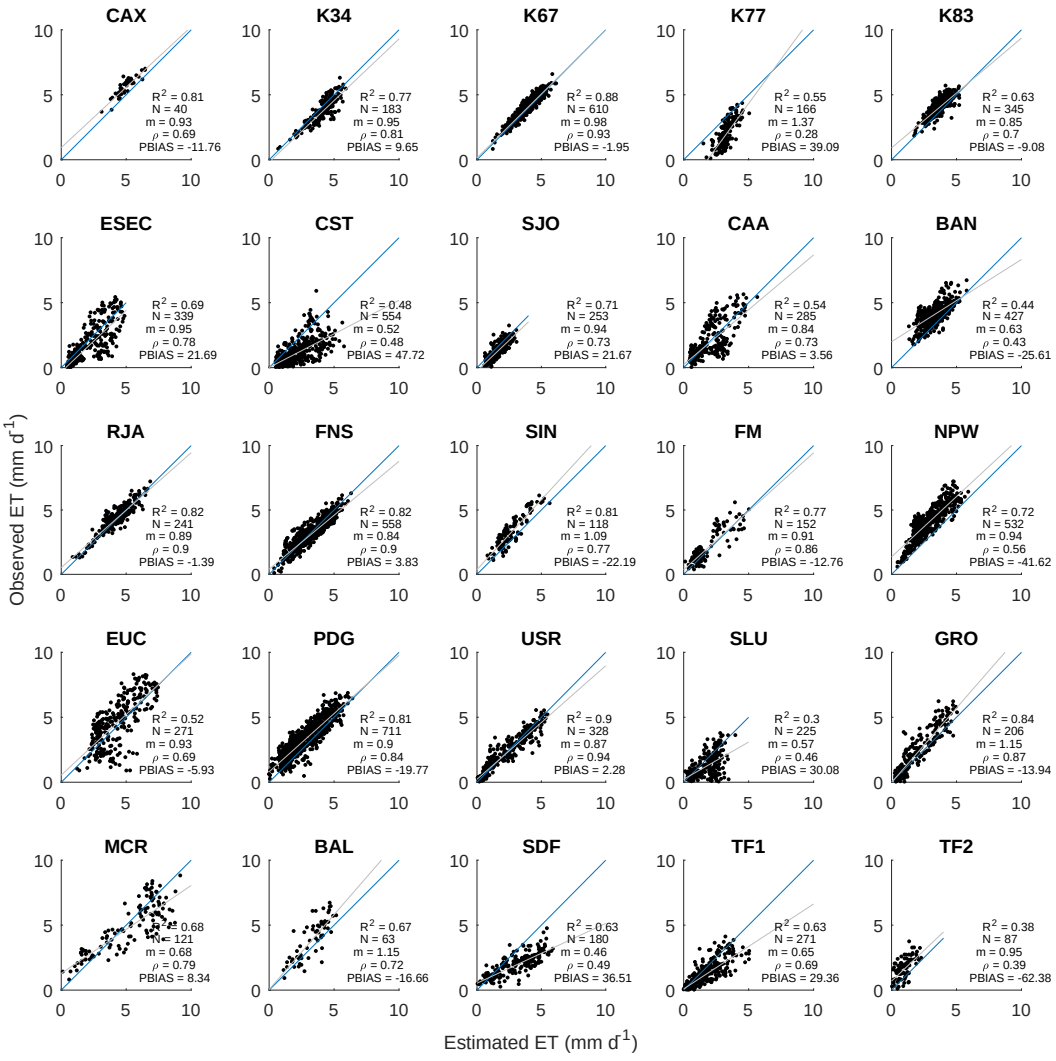

Figure 5. Comparison between observed and simulated ET from the PT-JPL model. N = sample size; R^2= determination coefficient, m = slope of the least squares regression line, ρ = concordance correlation coefficient, PBIAS = percent bias.

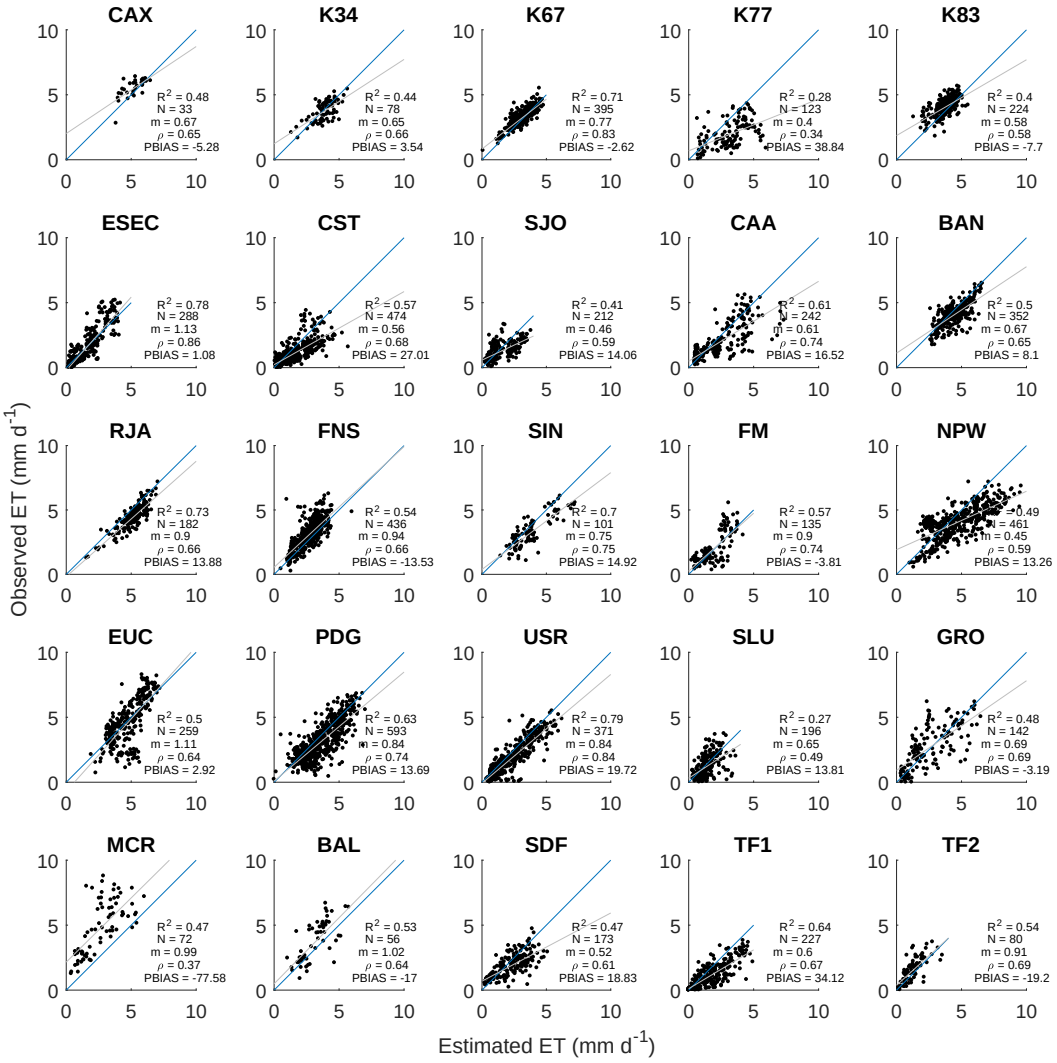

Figure 6. Comparison between observed and simulated ET from the PM-MOD model. N = sample size; R^2= determination coefficient, m = slope of the least squares regression line, ρ = concordance correlation coefficient, PBIAS = percent bias.

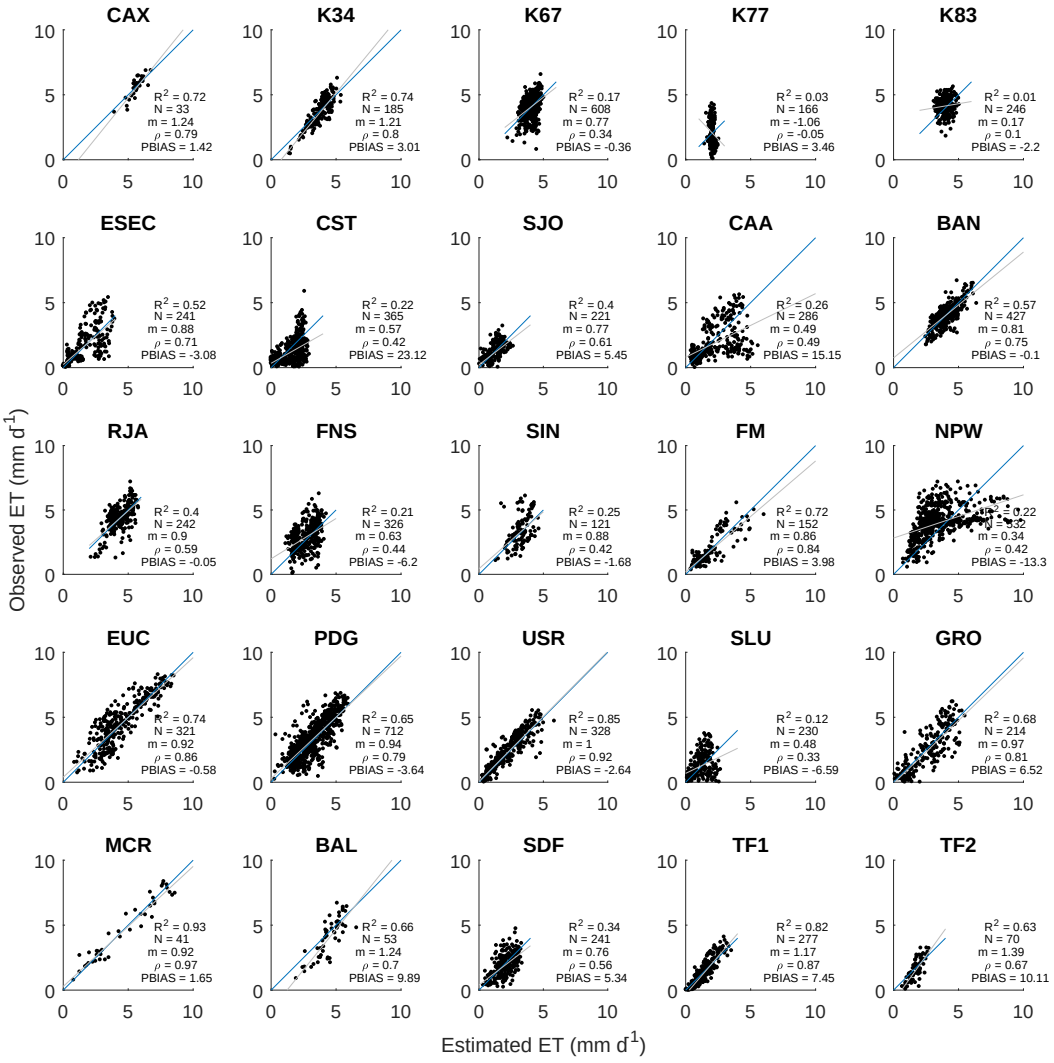

Figure 7. Comparison between observed and simulated ET from the PM-VI model. N = sample size; R^2= determination coefficient, m = slope of the least squares regression line, ρ = concordance correlation coefficient, PBIAS = percent bias.

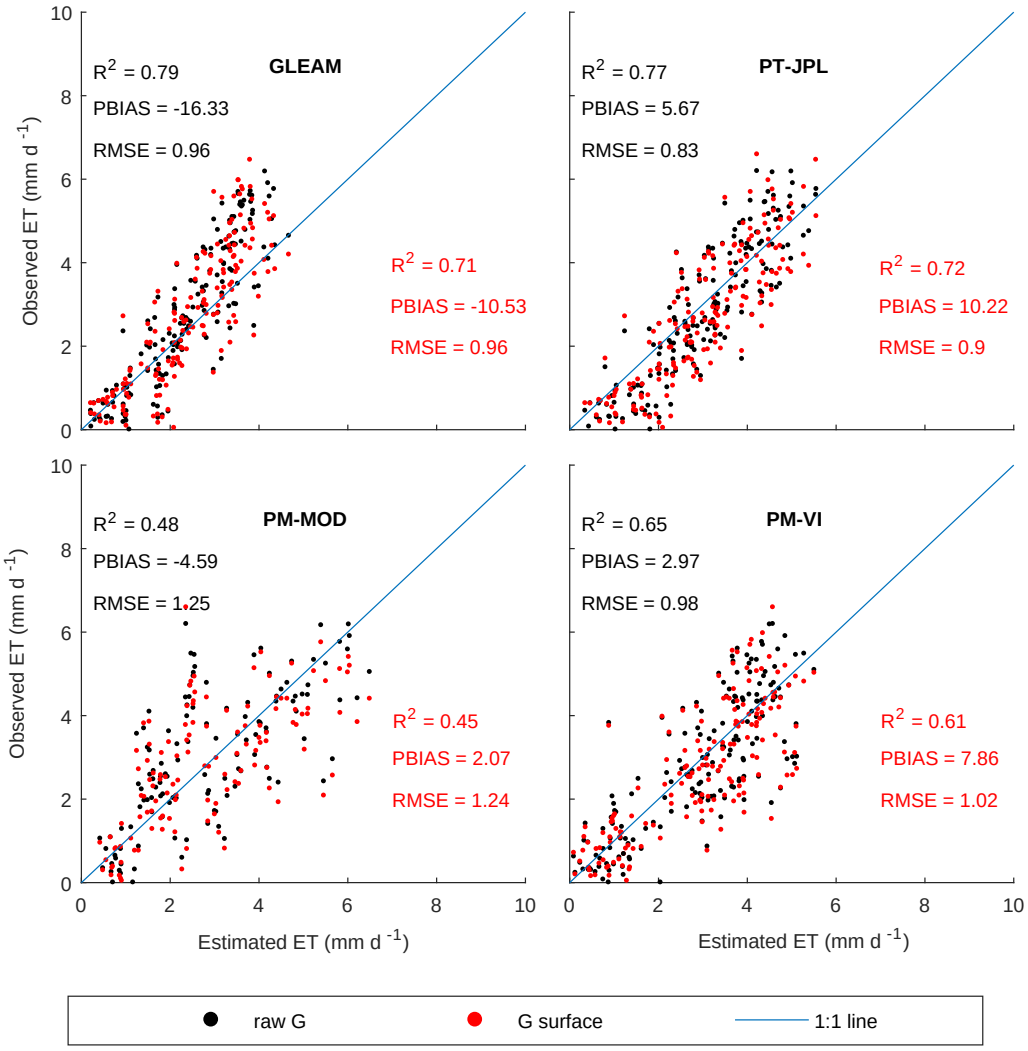

Figure 8. Comparison between observed and simulated *ET* with and without correcting *G*.

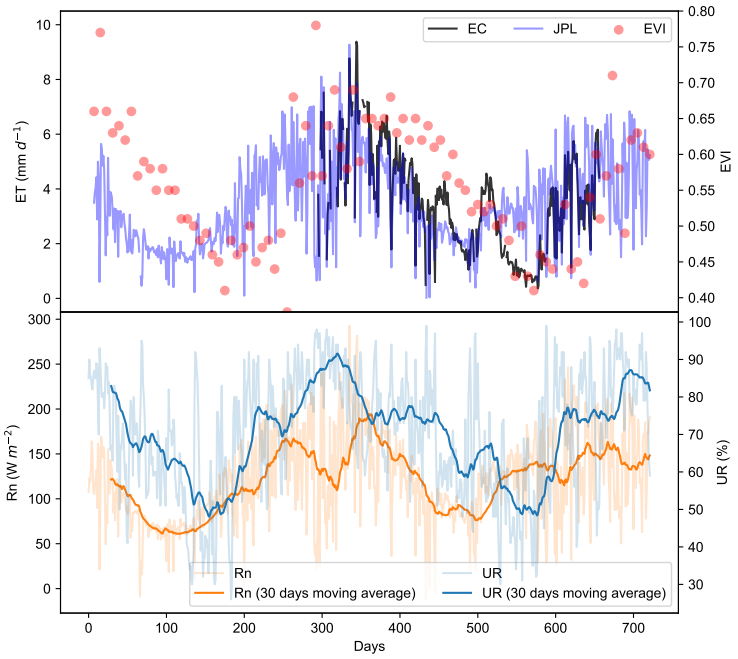

Figure 9. Relationship between observed ET (EC), simulated ET from PT-JPL and key meteorological variables at EUC site.

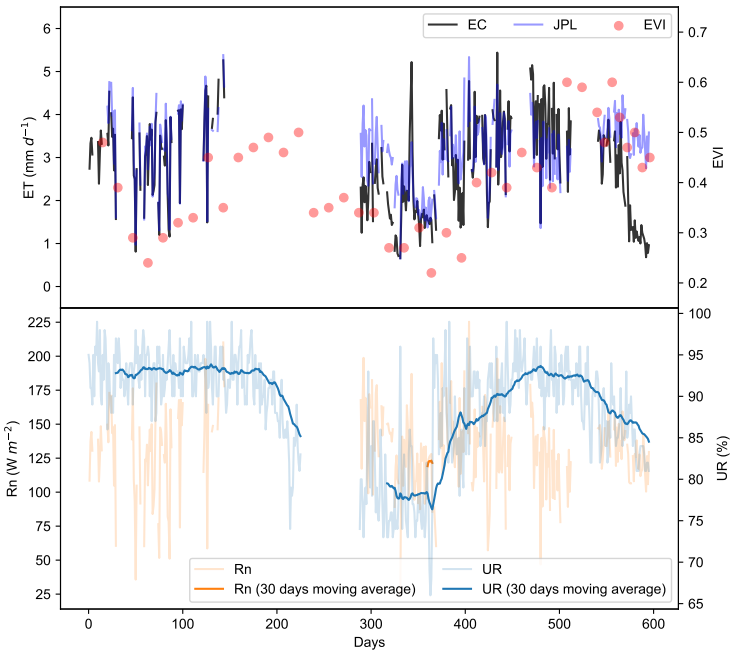

Figure 10. Relationship between observed ET (EC), simulated ET from PT-JPL and key meteorological variables at K77 site.

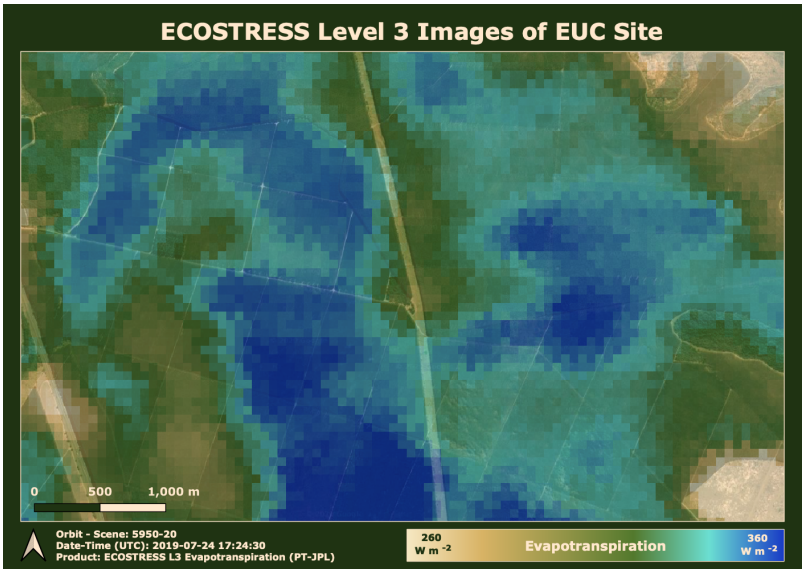

Figure 11. ECOSTRESS image (70-m resolution) for the EUC tower site

Tables S1-S3

Table 1. Description and characteristics of the biomes covered in this study.

Biome	Major ecoregion	Approximate area ($\times 10^3$ km^2)	Dominant climates
Tropical & Subtropical Moist Broadleaf Forests (TSMBF)	Amazon and Atlantic rainforests	8,750	Tropical Rainforest and Monsoon (Af and Am)
Tropical & Subtropical Dry Broadleaf Forests (TSDBF)	Caatinga and Chiquitano dry forests	1,000	Arid Steppe Hot (BSh)
Tropical & Subtropical Grasslands, Savannas & Shrublands (TSGSS)	Cerrado, Dry and Humid chaco, and Uruguayan savanna	4,250	Tropical Savanna (Aw)
Flooded Grasslands & Savannas (FGS)	Pantanal, Paraná flooded savanna, and Southern Cone Mesopotamian savanna	265	Tropical Savanna (Aw)
Temperate Broadleaf & Mixed Forests biome (TBMF)	Valdivian temperate forests and Magellanic subpolar forests	550	Temperate without dry season and warm summer (Cfb) and Polar Tundra (Td)
Temperate Grasslands, Savannas & Shrublands (TGSS)	Humid Pampas and Low Monte	576	Cold semi-arid (BSk) and Humid subtropical (Cfa)

Table 2. Flux towers used to validate remote sensing-based ET. Biome types: Tropical & Subtropical Moist Broadleaf Forests (TSMBF); Tropical & Subtropical Dry Broadleaf Forests (TSDBF); Temperate Broadleaf & Mixed Forests (TBMF); Tropical & Subtropical Grasslands, Savannas & Shrublands (TSGSS); Temperate Grasslands, Savannas & Shrublands (TGSS); Flooded Grasslands & Savannas (FGS). Land use classes: Evergreen Broadleaf Forest (EBF); Deciduous Broadleaf Forest (DBF); Grassland (GRA); Cropland (CROP); Woodland Savanna (WS), Mixed Forest (MF); Deciduous Needleleaf Forest (DNF); Permanent Wetland (PW). LULC = Land use/Land Cover. EBR = Energy Balance Ratio ($(LE + H)/(Rn - G)$). NA = not available

Name	Lat	Lon	Biome/LULC	Elevation (m)	EBR	Ref.
SDF	-41.88	-73.68	TBMF/EBF	50	NA	NA
K34	-2.61	-60.21	TSMBF/EBF	90	0.86	*Hutyra et al.* [2007]
RJA	-10.08	-61.93	TSMBF/DBF	180	0.74	*von Randow et al.* [2004]
CAX	-1.72	-51.46	TSMBF/EBF	57	NA	NA
FNS	-10.77	-62.34	TSMBF/GRA	240	0.77	*Hasler and Avissar* [2007]
K67	-2.86	-54.96	TSMBF/EBF	194	0.97	*Paca et al.* [2019]
K83	-3.02	-54.97	TSMBF/EBF	181	0.95	*Paca et al.* [2019]
K77	-3.01	-54.54	TSMBF/CROP	101	1.16	*Paca et al.* [2019]
SIN	-11.41	-55.32	TSMBF/WS	349	0.88	*Vourlitis et al.* [2008]
BAN	-9.82	-50.16	TSGSS/WS	168	0.9	*Borma et al.* [2009]
TF1	-54.97	-66.73	TBMF/PW	40	NA	*Kutzbach* [2019a]
TF2	-54.83	-68.45	TBMF/PW	60	NA	*Kutzbach* [2019b]
EUC	-21.58	-47.6	TSGSS/CROP	710	1.02	*Cabral et al.* [2011]
PDG	-21.62	-47.63	TSGSS/WS	710	0.99	*Cabral et al.* [2015]
USR	-21.64	-47.79	TSGSS/CROP	541	0.97	*Cabral et al.* [2012]
NPW	-16.49	-56.41	FGS/WS	120	NA	*Dalmagro et al.* [2018]
FM	-15.72	-56.07	TSGSS/MF	154	0.74	*Rodrigues et al.* [2014]
MCR	-37.55	-57.3	TGSS/PW	1	NA	*Tonti et al.* [2018]
GRO	-35.62	-61.32	TGSS/CROP	80	NA	NA
BAL	-37.75	-58.34	TGSS/CROP	130	NA	*Curto et al.* [2019]
SJO	-8.81	-36.41	TSDBF/GRA	702	0.96	*Machado et al.* [2016]
CST	-7.96	-38.38	TSDBF/DNF	468	0.73	*Souza et al.* [2015]
ESEC	-6.58	-37.25	TSDBF/DNF	205	0.87	*Campos et al.* [2019]
CAA	-9.05	-40.32	TSDBF/DNF	391	0.75	*Silva et al.* [2017]
SLU	-33.46	-66.46	TGSS/MF	320	0.86	*García et al.* [2017]

Table 3. Flux towers used to validate remote sensing-based ET. Biome types: Tropical & Subtropical Moist Broadleaf Forests (TSMBF); Tropical & Subtropical Dry Broadleaf Forests (TSDBF); Temperate Broadleaf & Mixed Forests (TBMF); Tropical & Subtropical Grasslands, Savannas & Shrublands (TSGSS); Temperate Grasslands, Savannas & Shrublands (TGSS); Flooded Grasslands & Savannas (FGS). Land use classes: Evergreen Broadleaf Forest (EBF); Deciduous Broadleaf Forest (DBF); Grassland (GRA); Cropland (CROP); Woodland Savanna (WS), Mixed Forest (MF); Deciduous Needleleaf Forest (DNF); Permanent Wetland (PW). LULC = Land use/Land Cover. EBR = Energy Balance Ratio ($(LE + H)/(Rn - G)$). NA = not available

Variable	Source of Product	Spatial resolution	Temporal resolution	Used by model
Air temperature (T)	Tower data	-	30 min	All
Downward shortwave radiation ($Rgs\downarrow$)	Tower data	-	30 min	PM-models
Surface outgoing radiation	Tower data	-	30 min	GLEAM
Net radiation (Rn)	Tower data	-	30 min	PT-models
Air pressure (P_{atm})	Tower data or calculated from ground elevation	-	30 min	PM-models
Precipitation (P)	Tower data	-	30 min	GLEAM
Vapor pressure (e_a)	Tower data	-	30 min	PM-models and PT-JPL
Air humidty (RH)	Tower data	-	30 min	PM-models
Wind speed	Tower data	-	30 min	PM-VI
Enhanced Vegetation Index (EVI)	MOD13Q1	250 m	16 days	PT-JPL and PM-VI
Vegetation Optical Depth (VOD)	TMI, SSM/I and AMSR-E	0.25°	16 days	GLEAM
Leaf area index (LAI)	MCD15A2H	500 m	8 days	PM-MOD
f_{PAR}	MCD15A2H	500 m	8 days	PM-MOD
albedo (α)	MCD43A3	500 m	daily	PM-MOD

References

Allen, R. G., L. S. Pereira, D. Raes, and M. Smith (1998), *Crop evapotranspiration - Guidelines for computing crop water requirements - FAO Irrigation and drainage paper 56*, FAO - Food and Agriculture Organization of the United Nations, Rome.

Aragon, B., R. Houborg, K. Tu, J. B. Fisher, and M. McCabe (2018), CubeSats Enable High Spatiotemporal Retrievals of Crop-Water Use for Precision Agriculture, *Remote Sensing*, *10*(12), 1867, doi:10.3390/rs10121867, number: 12 Publisher: Multidisciplinary Digital Publishing Institute.

Arroyo, M. T. K., P. Pliscoff, M. Mihoc, and M. Arroyo-Kalin (2005), The Magellanic moorland, in *The World's Largest Wetlands: Ecology and Conservation*, edited by L. H. Fraser and P. A. Keddy, pp. 424–445, Cambridge University Press, Cambridge, doi: 10.1017/CBO9780511542091.013.

Bai, J., L. Jia, S. Liu, Z. Xu, G. Hu, M. Zhu, and L. Song (2015), Characterizing the Footprint of Eddy Covariance System and Large Aperture Scintillometer Measurements to Validate Satellite-Based Surface Fluxes, *IEEE Geoscience and Remote Sensing Letters*, *12*(5), 943–947, doi:10.1109/LGRS.2014.2368580, conference Name: IEEE Geoscience and Remote Sensing Letters.

Borma, L. S., H. R. d. Rocha, O. M. Cabral, C. v. Randow, E. Collicchio, D. Kurzatkowski, P. J. Brugger, H. Freitas, R. Tannus, L. Oliveira, C. D. Rennó, and P. Artaxo (2009), Atmosphere and hydrological controls of the evapotranspiration over a floodplain forest in the Bananal Island region, Amazonia, *Journal of Geophysical Research: Biogeosciences*, *114*(G1), doi:10.1029/2007JG000641, _eprint: https://agupubs.onlinelibrary.wiley.com/doi/pdf/10.1029/2007JG000641.

Cabral, O. M. R., H. R. Rocha, J. H. C. Gash, M. A. V. Ligo, H. C. Freitas, and J. D. Tatsch (2010), The energy and water balance of a Eucalyptus plantation in southeast Brazil, *Journal of Hydrology*, *388*(3), 208–216, doi:10.1016/j.jhydrol.2010.04.041.

Cabral, O. M. R., J. H. C. Gash, H. R. Rocha, C. Marsden, M. A. V. Ligo, H. C. Freitas, J. D. Tatsch, and E. Gomes (2011), Fluxes of CO2 above a plantation of Eucalyptus in southeast Brazil, *Agricultural and Forest Meteorology*, *151*(1), 49–59, doi: 10.1016/j.agrformet.2010.09.003.

Cabral, O. M. R., H. R. Rocha, J. H. Gash, M. A. V. Ligo, J. D. Tatsch, H. C. Freitas, and E. Brasilio (2012), Water use in a sugarcane plantation, *GCB Bioenergy*, *4*(5), 555–565, doi:10.1111/j.1757-1707.2011.01155.x, _eprint:

https://onlinelibrary.wiley.com/doi/pdf/10.1111/j.1757-1707.2011.01155.x.

Cabral, O. M. R., H. R. da Rocha, J. H. Gash, H. C. Freitas, and M. A. V. Ligo (2015), Water and energy fluxes from a woodland savanna (cerrado) in southeast Brazil, *Journal of Hydrology: Regional Studies*, *4*, 22–40, doi:10.1016/j.ejrh.2015.04.010.

Campos, S., K. R. Mendes, L. L. da Silva, P. R. Mutti, S. S. Medeiros, L. B. Amorim, C. A. C. dos Santos, A. M. Perez-Marin, T. M. Ramos, T. V. Marques, P. S. Lucio, G. B. Costa, C. M. Santos e Silva, and B. G. Bezerra (2019), Closure and partitioning of the energy balance in a preserved area of a Brazilian seasonally dry tropical forest, *Agricultural and Forest Meteorology*, *271*, 398–412, doi:10.1016/j.agrformet.2019.03.018.

Chen, B., T. A. Black, N. C. Coops, T. Hilker, J. A. (Tony) Trofymow, and K. Morgenstern (2009), Assessing Tower Flux Footprint Climatology and Scaling Between Remotely Sensed and Eddy Covariance Measurements, *Boundary-Layer Meteorology*, *130*(2), 137–167, doi:10.1007/s10546-008-9339-1.

Costanza, R., R. d'Arge, R. de Groot, S. Farber, M. Grasso, B. Hannon, K. Limburg, S. Naeem, R. V. O'Neill, J. Paruelo, R. G. Raskin, P. Sutton, and M. van den Belt (1997), The value of the world's ecosystem services and natural capital, *Nature*, *387*(6630), 253–260, doi:10.1038/387253a0, number: 6630 Publisher: Nature Publishing Group.

Curto, L., M. Covi, and M. I. Gassmann (2019), Actual evapotranspiration and the pattern of soil water extraction of a soybean (Glycine max) crop, *Revista de la Facultad de Ciencias Agrarias UNCuyo*, *51*(2), 125–141, number: 2.

Dalmagro, H. J., M. J. Lathuillière, I. Hawthorne, D. D. Morais, O. B. Pinto Jr, E. G. Couto, and M. S. Johnson (2018), Carbon biogeochemistry of a flooded Pantanal forest over three annual flood cycles, *Biogeochemistry*, *139*(1), 1–18, doi:10.1007/s10533-018-0450-1.

de Queiroz, M. G., T. G. F. da Silva, S. Zolnier, C. A. A. de Souza, L. S. B. de Souza, G. do Nascimento Araújo, A. M. d. R. F. Jardim, and M. S. B. de Moura (2020), Partitioning of rainfall in a seasonal dry tropical forest, *Ecohydrology & Hydrobiology*, *20*(2), 230–242, doi:10.1016/j.ecohyd.2020.02.001.

Denmead, O. T., C. L. Mayocchi, and F. X. Dunin (1997), Does green cane harvesting conserve soil water?

Eltahir, E. a. B., and R. L. Bras (1994), Precipitation recycling in the Amazon basin, *Quarterly Journal of the Royal Meteorological Society*, *120*(518), 861–880, publisher: John Wiley & Sons, Ltd.

Embry, J. L., and E. A. Nothnagel (1994), Leaf Senescence of Postproduction Poinsettias in Low-light Stress, *Journal of the American Society for Horticultural Science*, *119*(5), 1006–1013, doi:10.21273/JASHS.119.5.1006, publisher: American Society for Horticultural Science Section: Journal of the American Society for Horticultural Science.

Ershadi, A., M. F. McCabe, J. P. Evans, and E. F. Wood (2015), Impact of model structure and parameterization on Penman–Monteith type evaporation models, *Journal of Hydrology*, *525*, 521–535, doi:10.1016/j.jhydrol.2015.04.008.

Fisher, J. B., K. P. Tu, and D. D. Baldocchi (2008), Global estimates of the land–atmosphere water flux based on monthly AVHRR and ISLSCP-II data, validated at 16 FLUXNET sites, *Remote Sensing of Environment*, *112*(3), 901–919, doi:10.1016/j.rse.2007.06.025.

Fisher, J. B., B. Lee, A. J. Purdy, G. H. Halverson, M. B. Dohlen, K. Cawse-Nicholson, A. Wang, R. G. Anderson, B. Aragon, M. A. Arain, D. D. Baldocchi, J. M. Baker, H. Barral, C. J. Bernacchi, C. Bernhofer, S. C. Biraud, G. Bohrer, N. Brunsell, B. Cappelaere, S. Castro-Contreras, J. Chun, B. J. Conrad, E. Cremonese, J. Demarty, A. R. Desai, A. D. Ligne, L. Foltýnová, M. L. Goulden, T. J. Griffis, T. Grünwald, M. S. Johnson, M. Kang, D. Kelbe, N. Kowalska, J.-H. Lim, I. Maïnassara, M. F. McCabe, J. E. C. Missik, B. P. Mohanty, C. E. Moore, L. Morillas, R. Morrison, J. W. Munger, G. Posse, A. D. Richardson, E. S. Russell, Y. Ryu, A. Sanchez-Azofeifa, M. Schmidt, E. Schwartz, I. Sharp, L. Šigut, Y. Tang, G. Hulley, M. Anderson, C. Hain, A. French, E. Wood, and S. Hook (2020), ECOSTRESS: NASA's Next Generation Mission to Measure Evapotranspiration From the International Space Station, *Water Resources Research*, *56*(4), e2019WR026,058, doi:10.1029/2019WR026058, _eprint: https://agupubs.onlinelibrary.wiley.com/doi/pdf/10.1029/2019WR026058.

García, A. G., C. M. Di Bella, J. Houspanossian, P. N. Magliano, E. G. Jobbágy, G. Posse, R. J. Fernández, and M. D. Nosetto (2017), Patterns and controls of carbon dioxide and water vapor fluxes in a dry forest of central Argentina, *Agricultural and Forest Meteorology*, *247*, 520–532, doi:10.1016/j.agrformet.2017.08.015.

García, M., I. Sandholt, P. Ceccato, M. Ridler, E. Mougin, L. Kergoat, L. Morillas, F. Timouk, R. Fensholt, and F. Domingo (2013), Actual evapotranspiration in drylands derived from in-situ and satellite data: Assessing biophysical constraints, *Remote Sensing of Environment*, *131*, 103–118, doi:10.1016/j.rse.2012.12.016.

Gash, J. H. C., C. R. Lloyd, and G. Lachaud (1995), Estimating sparse forest rainfall interception with an analytical model, *Journal of Hydrology*, *170*(1), 79–86, doi:10.1016/0022-

1694(95)02697-N.

Hasler, N., and R. Avissar (2007), What Controls Evapotranspiration in the Amazon Basin?, *Journal of Hydrometeorology*, *8*(3), 380–395, doi:10.1175/JHM587.1, publisher: American Meteorological Society.

Hutyra, L. R., J. W. Munger, S. R. Saleska, E. Gottlieb, B. C. Daube, A. L. Dunn, D. F. Amaral, P. B. d. Camargo, and S. C. Wofsy (2007), Seasonal controls on the exchange of carbon and water in an Amazonian rain forest, *Journal of Geophysical Research: Biogeosciences*, *112*(G3), doi:10.1029/2006JG000365, _eprint: https://agupubs.onlinelibrary.wiley.com/doi/pdf/10.1029/2006JG000365.

Jasechko, S., Z. D. Sharp, J. J. Gibson, S. J. Birks, Y. Yi, and P. J. Fawcett (2013), Terrestrial water fluxes dominated by transpiration, *Nature*, *496*(7445), 347–350, doi:10.1038/nature11983, number: 7445 Publisher: Nature Publishing Group.

Junk, W. J., M. Brown, I. C. Campbell, M. Finlayson, B. Gopal, L. Ramberg, and B. G. Warner (2006a), The comparative biodiversity of seven globally important wetlands: a synthesis, *Aquatic Sciences*, *68*(3), 400–414, doi:10.1007/s00027-006-0856-z.

Junk, W. J., C. N. da Cunha, K. M. Wantzen, P. Petermann, C. Strüssmann, M. I. Marques, and J. Adis (2006b), Biodiversity and its conservation in the Pantanal of Mato Grosso, Brazil, *Aquatic Sciences*, *68*(3), 278–309, doi:10.1007/s00027-006-0851-4.

Kutzbach, L. (2019a), Lars Kutzbach (2019), AmeriFlux AR-TF1 Rio Moat bog, Ver. 1-5, AmeriFlux AMP, (Dataset), doi:https://doi.org/10.17190/AMF/1543389.

Kutzbach, L. (2019b), Lars Kutzbach (2019), AmeriFlux AR-TF2 Rio Pipo bog, Ver. 1-5, AmeriFlux AMP, (Dataset), doi:https://doi.org/10.17190/AMF/1543388.

Machado, C. B., J. R. d. S. Lima, A. C. D. Antonino, E. S. d. Souza, R. M. S. Souza, E. M. Alves, C. B. Machado, J. R. d. S. Lima, A. C. D. Antonino, E. S. d. Souza, R. M. S. Souza, and E. M. Alves (2016), Daily and seasonal patterns of CO2 fluxes and evapotranspiration in maize-grass intercropping, *Revista Brasileira de Engenharia Agrícola e Ambiental*, *20*(9), 777–782, doi:10.1590/1807-1929/agriambi.v20n9p777-782, publisher: Departamento de Engenharia Agrícola - UFCG / Cnpq.

Marques, T. V., K. Mendes, P. Mutti, S. Medeiros, L. Silva, A. M. Perez-Marin, S. Campos, P. S. Lúcio, K. Lima, J. dos Reis, T. M. Ramos, D. F. da Silva, C. P. Oliveira, G. B. Costa, A. C. D. Antonino, R. S. C. Menezes, C. M. Santos e Silva, and B. Bezerra (2020), Environmental and biophysical controls of evapotranspiration from Seasonally Dry Tropical Forests (Caatinga) in the Brazilian Semiarid, *Agricultural and Forest Meteorology*, *287*,

107,957, doi:10.1016/j.agrformet.2020.107957.

McCabe, M. F., A. Ershadi, C. Jimenez, D. G. Miralles, D. Michel, and E. F. Wood (2016), The GEWEX LandFlux project: evaluation of model evaporation using tower-based and globally gridded forcing data, *Geoscientific Model Development*, *9*(1), 283–305, doi: https://doi.org/10.5194/gmd-9-283-2016.

Mu, Q., M. Zhao, and S. W. Running (2011), Improvements to a MODIS global terrestrial evapotranspiration algorithm, *Remote Sensing of Environment*, *115*(8), 1781–1800, doi: 10.1016/j.rse.2011.02.019.

Mutti, P. R., L. L. da Silva, S. d. S. Medeiros, V. Dubreuil, K. R. Mendes, T. V. Marques, P. S. Lúcio, C. M. Santos e Silva, and B. G. Bezerra (2019), Basin scale rainfall-evapotranspiration dynamics in a tropical semiarid environment during dry and wet years, *International Journal of Applied Earth Observation and Geoinformation*, *75*, 29–43, doi: 10.1016/j.jag.2018.10.007.

Myers, N., R. A. Mittermeier, C. G. Mittermeier, G. A. B. d. Fonseca, and J. Kent (2000), Biodiversity hotspots for conservation priorities, *Nature*, *403*(6772), 853–858, doi: 10.1038/35002501.

Nagler, P. L., J. Cleverly, E. Glenn, D. Lampkin, A. Huete, and Z. Wan (2005), Predicting riparian evapotranspiration from MODIS vegetation indices and meteorological data, *Remote Sensing of Environment*, *94*(1), 17–30, doi:10.1016/j.rse.2004.08.009.

Paca, V. H. d. M., G. E. Espinoza-Dávalos, T. M. Hessels, D. M. Moreira, G. F. Comair, and W. G. M. Bastiaanssen (2019), The spatial variability of actual evapotranspiration across the Amazon River Basin based on remote sensing products validated with flux towers, *Ecological Processes*, *8*(1), 6, doi:10.1186/s13717-019-0158-8.

Rodrigues, T. R., G. L. Vourlitis, F. d. A. Lobo, R. G. d. Oliveira, and J. d. S. Nogueira (2014), Seasonal variation in energy balance and canopy conductance for a tropical savanna ecosystem of south central Mato Grosso, Brazil, *Journal of Geophysical Research: Biogeosciences*, *119*(1), 1–13, doi:10.1002/2013JG002472, _eprint: https://agupubs.onlinelibrary.wiley.com/doi/pdf/10.1002/2013JG002472.

Silva, P. F. d., J. R. d. S. Lima, A. C. D. Antonino, R. Souza, E. S. d. Souza, J. R. I. Silva, and E. M. Alves (2017), Seasonal patterns of carbon dioxide, water and energy fluxes over the Caatinga and grassland in the semi-arid region of Brazil, *Journal of Arid Environments*, *147*, 71–82, doi:10.1016/j.jaridenv.2017.09.003.

Souza, L. S. B. d., M. S. B. d. Moura, G. C. Sediyama, T. G. F. d. Silva, L. S. B. d. Souza, M. S. B. d. Moura, G. C. Sediyama, and T. G. F. d. Silva (2015), Balanço de energia e controle biofísico da evapotranspiração na Caatinga em condições de seca intensa, *Pesquisa Agropecuária Brasileira*, *50*(8), 627–636, doi:10.1590/S0100-204X2015000800001, publisher: Embrapa Informação Tecnológica.

Stoy, P. C., T. S. El-Madany, J. B. Fisher, P. Gentine, T. Gerken, S. P. Good, A. Klosterhalfen, S. Liu, D. G. Miralles, O. Perez-Priego, A. J. Rigden, T. H. Skaggs, G. Wohlfahrt, R. G. Anderson, A. M. J. Coenders-Gerrits, M. Jung, W. H. Maes, I. Mammarella, M. Mauder, M. Migliavacca, J. A. Nelson, R. Poyatos, M. Reichstein, R. L. Scott, and S. Wolf (2019), Reviews and syntheses: Turning the challenges of partitioning ecosystem evaporation and transpiration into opportunities, *Biogeosciences*, *16*(19), 3747–3775, doi:10.5194/bg-16-3747-2019, publisher: Copernicus GmbH.

Tetens, O. (1930), *Über einige meteorologische Begriffe*, Friedrich Vieweg & Sohn Akt.-Gesellschaft.

Tonti, N. E., M. I. Gassmann, and C. F. Pérez (2018), First results of energy and mass exchange in a salt marsh on southeastern South America, *Agricultural and Forest Meteorology*, *263*, 59–68, doi:10.1016/j.agrformet.2018.08.001.

Valente, F., J. S. David, and J. H. C. Gash (1997), Modelling interception loss for two sparse eucalypt and pine forests in central Portugal using reformulated Rutter and Gash analytical models, *Journal of Hydrology*, *190*(1), 141–162, doi:10.1016/S0022-1694(96)03066-1.

von Randow, C., A. O. Manzi, B. Kruijt, P. J. de Oliveira, F. B. Zanchi, R. L. Silva, M. G. Hodnett, J. H. C. Gash, J. A. Elbers, M. J. Waterloo, F. L. Cardoso, and P. Kabat (2004), Comparative measurements and seasonal variations in energy and carbon exchange over forest and pasture in South West Amazonia, *Theoretical and Applied Climatology*, *78*(1), 5–26, doi:10.1007/s00704-004-0041-z.

Vourlitis, G. L., J. d. S. Nogueira, F. d. A. Lobo, K. M. Sendall, S. R. d. Paulo, C. A. A. Dias, O. B. Pinto, and N. L. R. d. Andrade (2008), Energy balance and canopy conductance of a tropical semi-deciduous forest of the southern Amazon Basin, *Water Resources Research*, *44*(3), doi:10.1029/2006WR005526, _eprint: https://agupubs.onlinelibrary.wiley.com/doi/pdf/10.1029/2006WR005526.

Wardlow, B. D., S. L. Egbert, and J. H. Kastens (2007), Analysis of time-series MODIS 250 m vegetation index data for crop classification in the U.S. Central Great Plains, *Remote Sensing of Environment*, *108*(3), 290–310, doi:10.1016/j.rse.2006.11.021.

Wei, Z., K. Yoshimura, L. Wang, D. G. Miralles, S. Jasechko, and X. Lee (2017), Revisiting the contribution of transpiration to global terrestrial evapotranspiration, *Geophysical Research Letters*, *44*(6), 2792–2801, doi:https://doi.org/10.1002/2016GL072235, _eprint: https://agupubs.onlinelibrary.wiley.com/doi/pdf/10.1002/2016GL072235.

Zhou, S., B. Yu, Y. Zhang, Y. Huang, and G. Wang (2016), Partitioning evapotranspiration based on the concept of underlying water use efficiency, *Water Resources Research*, *52*(2), 1160–1175, doi:10.1002/2015WR017766, _eprint: https://agupubs.onlinelibrary.wiley.com/doi/pdf/10.1002/2015WR017766.